Frequency of Proterozoic geomagnetic superchrons

Peter E. Driscoll [a,*], David A.D. Evans [b]

[a] *Department of Terrestrial Magnetism, Carnegie Institution for Science, 5241 Broad Branch Rd., Washington, DC 20015-1305, USA*
[b] *Department of Geology & Geophysics, Yale University, 210 Whitney Avenue, New Haven, CT 06520, USA*

A B S T R A C T

Long-term geodynamo evolution is expected to respond to inner core growth and changing patterns of mantle convection. Three geomagnetic superchrons, during which Earth's magnetic field maintained a near-constant polarity state through tens of Myr, are known from the bio/magnetostratigraphic record of Phanerozoic time, perhaps timed according to supercontinental episodicity. Some geodynamo simulations incorporating a much smaller inner core, as would have characterized Proterozoic time, produce field reversals at a much lower rate. Here we compile polarity ratios of site means within a quality-filtered global Proterozoic paleomagnetic database, according to recent plate kinematic models. Various smoothing parameters, optimized to successfully identify the known Phanerozoic superchrons, indicate 3–10 possible Proterozoic superchrons during the 1300 Myr interval studied. Proterozoic geodynamo evolution thus appears to indicate a relatively narrow range of reversal behavior through the last two billion years, implying either remarkable stability of core dynamics over this time or insensitivity of reversal rate to core evolution.

© 2016 Elsevier B.V. All rights reserved.

1. Introduction

In the paleomagnetic record, absolute polarity of the geodynamo can be established unambiguously if there exists, for each tectonic plate, a succession of closely spaced poles defining a continuous apparent polar wander path (APWP). For major continental blocks, the most recent synthesis of such paths (Torsvik et al., 2012), plus magnetostratigraphic studies of well-exposed volcano-sedimentary successions, allow for precise temporal control on reversals (Gradstein et al., 2004). Within that time interval there are three known superchrons: Cretaceous (N), Kiaman (R), and Moyero (R), where (N) and (R) refer to Normal and Reversed states of the field relative to the present. Among these, the Moyero is least well resolved due to sparseness of sampling outside the type Siberian magnetostratigraphic sections. Nonetheless, Phanerozoic superchrons have occurred with a frequency of about one per 200 Myr (Biggin et al., 2012).

Here we present a new Proterozoic global paleomagnetic database (Fig. 1, Supplementary Data Table 1) and compare statistics of its polarity ratio series to an updated Phanerozoic data set. Proterozoic volcano-sedimentary successions with complete preservation of primary magnetic remanence are rare. Possible su-

perchrons identified by magnetostratigraphy of such successions include: ca. 1000 Ma from Siberia ("Maya N", Pavlov and Gallet, 2010), ca. 1100–1085 Ma from central Laurentia ("Keweenawan N", Davis and Green, 1997), ca. 1460–1430 Ma from western Laurentia ("Middle Belt R", Elston et al., 2002), and ca. 1650–1590 Ma ("Upper McArthur", Idnurm et al., 1995). In addition, Irving et al. (2004) proposed a superchron at ca. 1760–1740 Ma ("Cleaver N") based on uniformity of polarity among magnetic overprints across the Canadian Shield. Gallet et al. (2012) propose that superchrons were more common during the Precambrian than the Phanerozoic based on the few continuous magnetostratigraphic data that indicate abrupt transitions from reversing to non-reversing states. Coe and Glatzmaier (2006) considered some of the proposed Proterozoic superchrons as evidence for more abundant superchron occurrence in early Earth history, but such an assertion lacks statistical rigor.

We aim to test these hypotheses with a global compilation of Proterozoic polarity ratios. We employ a polarity bias approach, assessing the entire global paleomagnetic database for abundances of one polarity over another, at the site-mean level. Our approach, broadly similar to that employed by previous analyses of Phanerozoic data (McElhinny, 1971; Irving and Pullaiah, 1976; Johnson et al., 1995; Algeo, 1996) and longer periods of Earth history (Irving et al., 1976; Roberts and Piper, 1989), is advantageous in allowing continuous future refinement because many high-quality paleomagnetic data derive from non-stratified rocks

---

such as mafic dyke swarms (Buchan, 2013). The disadvantage of our approach is that it cannot distinguish a truly non-reversing superchron from a prolonged interval of a dominant polarity with ephemeral opposite-polarity states; but even the three Phanerozoic superchrons likely contained brief reversed states (Gradstein et al., 2004).

The second limitation of Proterozoic paleomagnetic poles is their lack of connectivity to Phanerozoic APWPs, commonly disjointed through the problematic Ediacaran Period (Raub et al., 2007; Abrajevitch and Van der Voo, 2010; Halls et al., 2015). Nonetheless, long isolated strands of APWPs are available for some Proterozoic cratons, notably Laurentia (1800–950 Ma), Baltica (1750–900 Ma), and Australia (1800–1550 Ma). Prior to initial amalgamation of those cratons, some of their component cratons are also linked by APWP extension to as old as 1800 Ma (Sarmatia), 1900 Ma (Fennoscandia, Slave), or even 2200 Ma (Superior). Initial polarity analysis of only Laurentian data indicated a strong N-polarity bias at ca. 1000 Ma (Irving et al., 1976), and global analysis under the assumption of a particular supercontinent model showed pronounced N-polarity biases at ca. 1000 and 1700 Ma (Roberts and Piper, 1989). More recently, several plate kinematic models incorporating geological and paleomagnetic data have begun to assemble the Neoproterozoic Rodinia supercontinent (Li et al., 2013) and its Mesoproterozoic predecessor Nuna (Pisarevsky et al., 2014; Pehrsson et al., 2015) to first order. The relative positions of Laurentia, Baltica, Siberia, proto-Australia, and North China are the most consistently placed through the 1800–900 Ma interval, with only minor variations that do not affect interpretation of relative geomagnetic polarity. Principal differences among the most recent models apply to the placement of India, Amazonia, and West Africa, but those differences do not substantially influence our conclusions because reliable data from those blocks are sparse (Fig. 1). In addition to the globally merged relative polarity records, absolute geomagnetic polarity may be assigned according to trade-wind orographic patterns across Slave craton at ca. 1900 Ma and Laurentia at ca. 1100 Ma (Hoffman and Grotzinger, 1993), and consequently, APWP connectivity expands this polarity choice throughout the reconstructed global dataset.

The third limitation of the Proterozoic paleomagnetic database is the relative sparseness of high-quality data ($n_{avg} = 0.12$ poles/Myr), a sampling rate about a factor of eight lower than that of the Phanerozoic dataset ($n_{avg} = 0.92$ poles/Myr). In order to assess the significance of Proterozoic geomagnetic superchrons our analysis is tested with the Phanerozoic dataset compiled from a recent quality-filtered global kinematic analysis (Torsvik et al., 2012), which encompasses two, or perhaps three, superchrons known from seafloor spreading records (e.g. CNS, Lowrie and Kent, 2004) or magnetostratigraphic compilations (e.g. KRS and MRS, Pavlov and Gallet, 2005). Both datasets are subjected to a range of statistical smoothing that seek the "correct" or at least reproducible identification of superchrons.

2. Methods

To provide a standard measure of geomagnetic polarity bias across Proterozoic–Phanerozoic time, we apply bootstrap subsampling to the Phanerozoic global database at a variety of sampling densities n_{samp} (including its full value, a value equivalent to the Proterozoic, and an intermediate value; Table 1). In our analysis, we define a superchron as a continuous period with a smoothed polarity ratio within 20% of normal or reverse polarity for at least 15 Myr. To test sensitivity of time-averaging, we vary the smoothing window interval (τ) from 1 to 25 Myr; with a small τ the method may exclude legitimate superchrons because of full weight applied to short-lived but densely sampled opposite-polarity intervals within extended single-polarity periods, or with a large τ the
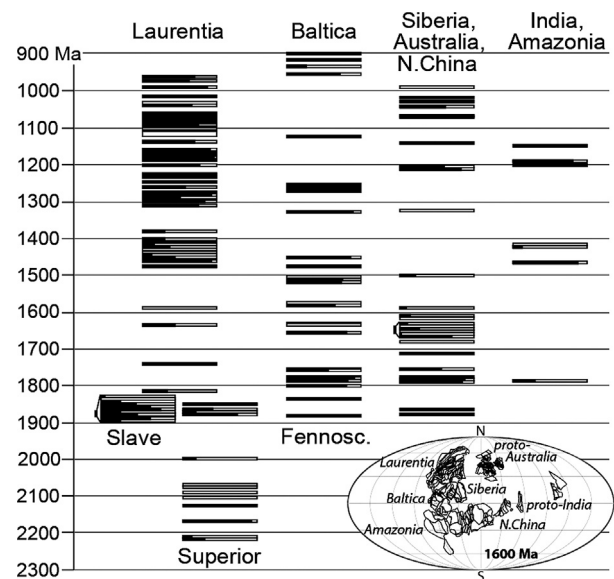

Fig. 1. Proterozoic geomagnetic polarity ratios from a global dataset merged according to the Nuna supercontinent reconstruction shown in the inset. Each bar represents a published paleomagnetic result (or compilation; Supplementary Data Table 1) with proportion of Normal (black) or Reversed (white) data.

Table 1
Summary of polarity ratio data sets where N is total number of polarity ratios in data set, Δt is the time span of the data set, and $n_{ave} = N/\Delta t$ is the sampling density.

Data set	N	Age range (Ma)	Δt (Myr)	n_{ave} (Myr^{-1})
Phanerozoic	505	0–550	550	0.918
Proterozoic	159	900–2219	1319	0.120

smoothed polarity ratio curve may exclude legitimate superchrons by averaging results from beyond their temporal limits.

We compile paleopole data from the global paleomagnetic database with strict quality criteria so that all the polarity ratio data included have at least 4 site means and age precision within ±15 Myr (a nominal superchron duration). Phanerozoic global paleomagnetic data are taken from Torsvik et al. (2012), and Proterozoic data are largely from Veikkolainen et al. (2014) and updated by the authors. For each pole, assignment of polarity bias on a site-mean level is checked manually for consistency with tectonic reconstructions; numerous discrepancies exist between our globally merged polarity selection and those of individual studies due to arbitrary conventions applied at local scales (e.g., Northern Hemisphere data are generally described as N polarity if remanence directions are downward).

The Phanerozoic polarity ratio sequence contains 505 polarity ratios over 550 Myr, corresponding to a sampling frequency of $n_{ave} = 0.92$ Myr^{-1} (Table 1). Our smoothing analysis broadly replicates that of Algeo (1996) and we employ the same inverse-distance squared smoothing function (see Appendix A). The mean polarity ratio of a frequently reversing dipole should be close to 50%, while superchron periods correlate with extreme values (0–20% or 80–100%). To quantify the statistical significance of a superchron identified in a polarity ratio series we generate an ensemble of polarity ratio sequences from the Phanerozoic and Proterozoic data sets for a chosen sampling density n_{samp}, apply a given smoothing window size τ, and search the smoothed sequence for superchrons using the criteria above. These superchrons are recorded and their statistics tabulated (Tables 2 and 3).

In the Phanerozoic where the ages of superchrons are known this is a test of the method, and an opportunity to distinguish po-

Table 2

Summary table of Phanerozoic bootstrap results in Fig. 3 for $\tau = 1$–25 Myr and minimum superchron length of 15 Myr. Chron denotes the superchron name (CNS = Cretaceous N Superchron, JGS = Jurassic Ghost Superchron, KRS = Kiaman Reverse Superchron, and MRS = Moyero Reverse Superchron). n_{samp} is the bootstrap sampling density per Myr. N_{SC} is the number of times the superchron was successfully identified out of 25 cases, each with different smoothing window size τ. The fraction of cases that identified the superchron is $f_{SC} = N_{SC}/25$. t_{lo} is the mean superchron start time and σ_{lo} is the standard deviation of t_{lo}. t_{len} is the mean superchron length and σ_{lo} is the standard deviation of t_{len} in Myr.

Chron	n_{samp}	N_{SC}	f_{SC}	Mean t_{lo} (σ_{lo})	Mean t_{len} (σ_{len})
CNS	0.91	6	0.24	85.3 (0.5)	27.9 (2.0)
CNS	0.50	14	0.56	87.6 (2.2)	25.7 (2.8)
CNS	0.12	25	1.00	85.3 (3.3)	38.0 (8.1)
JGS	0.91	0	0.00	0.0 (0.0)	0.0 (0.0)
JGS	0.50	10	0.40	175.5 (3.5)	23.6 (1.4)
JGS	0.12	24	0.96	156.7 (19.3)	42.8 (18.7)
KRS	0.91	25	1.00	264.0 (4.3)	54.8 (2.2)
KRS	0.50	25	1.00	264.6 (4.3)	52.2 (4.4)
KRS	0.12	25	1.00	266.3 (3.0)	51.0 (3.3)
MRS	0.91	0	0.00	0.0 (0.0)	0.0 (0.0)
MRS	0.50	17	0.68	488.7 (12.0)	39.3 (14.3)
MRS	0.12	25	1.00	475.5 (7.0)	54.6 (9.4)

Fig. 2. Polarity ratio data (squares) with temporally smoothed ($\tau = 7$ Myr) polarity ratio curve (solid) for Phanerozoic (left) and Proterozoic (right) paleomagnetic data. Dashed lines indicate one standard deviation from the running average (see Appendix A). Shading indicates superchron periods where the polarity ratio is extreme (either 0–20% or 80–100%).

tential false positives from real superchrons. Fig. 2(left) shows the Phanerozoic polarity ratio series with smoothing $\tau = 7$ Myr. The CNS and KRS are clearly identified, but the MRS at this τ is not. Below we explore how the superchron identification rate varies with polarity ratio sampling density n_{ave} and smoothing window size τ.

The Proterozoic polarity ratio sequence contains 159 poles over 1319 Myr, corresponding to a sampling frequency of $n_{ave} = 0.12$ Myr^{-1} (Table 1). Fig. 2(right) shows the Proterozoic polarity ratio series for a smoothing window of $\tau = 7$ Myr. Identification of superchrons in the Proterozoic sequence requires a statistical analysis of the data for a range of τ, and careful interpretation in light of the relatively well constrained Phanerozoic superchron occurrences. In the Proterozoic polarity ratio sequence this method identifies new superchrons (Table 3) and periods of extended polarity bias.

3. Results

3.1. Phanerozoic

We first apply the analysis to the Phanerozoic polarity ratio sequence in Fig. 2(left). For each combination of sampling density n_{samp} and smoothing window size τ we generate 100 Phanerozoic polarity ratio sequences subsampled at random from the full Phanerozoic sequence. Each sequence is then smoothed using an inverse-distance squared function (see Appendix A) and the mean and standard deviation of each superchron age and length over the

100 sequences is computed. Table 2 and Fig. 3 show the results of this analysis for $n_{samp} = 0.91$ (full Phanerozoic dataset), 0.5 (intermediate), and 0.12 (Proterozoic sampling rate) samples per Myr. At each sampling density a range of smoothing windows are used from $\tau = 1$ to 25 Myr, in 1 Myr increments. For each set of 100 bootstrap sequences analyzed, we compute the mean superchron ending age t_{lo} and standard deviation σ_{lo}, and mean superchron length t_{len} and standard deviation σ_{len} (Table 2, Fig. 3). We then compare the mean superchron occurrence time from these 100 sequences to the three known superchrons and consider the superchron to be successfully recovered if the mean superchron age span (t_{lo} to $t_{lo} + t_{len}$) includes the mid-age (halfway between the start and end) of a known superchron. The number of successfully recovered superchrons out of the 25 smoothing windows tested is N_{SC} and the recovery rate is $f_{SC} = N_{SC}/25$ (Table 2).

There are four main features in the Phanerozoic: the three known superchrons and a period of strong normal polarity bias in the Early Jurassic (also identified by Algeo, 1996). We refer to the Jurassic period of strong polarity bias as the "Jurassic Ghost Superchron" (JGS) as frequent reversals are known to have occurred during this time (Ogg, 2012). The presence of the JGS in the analysis is due to dense sampling of short-lived magmatic events emplaced during two brief N-polarity intervals associated with The Central Atlantic Magmatic Province (Blackburn et al., 2013; Burgess et al., 2015). Therefore the polarity bias is likely attributable to sampling bias and serves as a cautionary example for datasets that include high-density sampling of specific rock formations.

The KRS is easily identified over all sampling densities and smoothing windows considered, with the deviation of the ending age σ_{lo} always less than 10 Myr. The CNS is the next best-constrained superchron, however it is surprisingly identified more often with a low sampling density (Fig. 3 and Table 2). The devia-

Table 3

Summary table of Proterozoic analysis in Fig. 3 for $\tau = 1$–25 Myr and minimum superchron length of 15 Myr. N_{SC} is the number of times the superchron was successfully identified out of 25 τ cases. Mean and standard deviation of the superchron start time and length are t_{lo} and σ_{lo}, and t_{len} and σ_{len}, respectively, in Myr. The last three columns show superchron age using the start age and length computed from the mean of all τ, and the age range computed with $\tau = 1$ and 7 Myr, respectively. All ages in Ma.

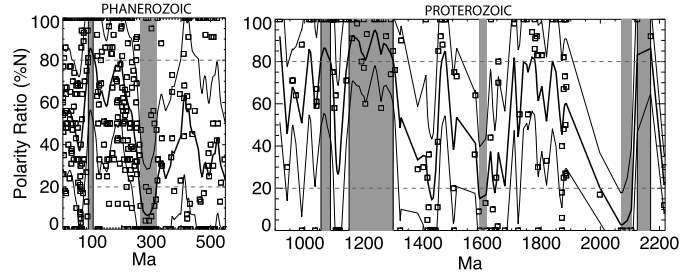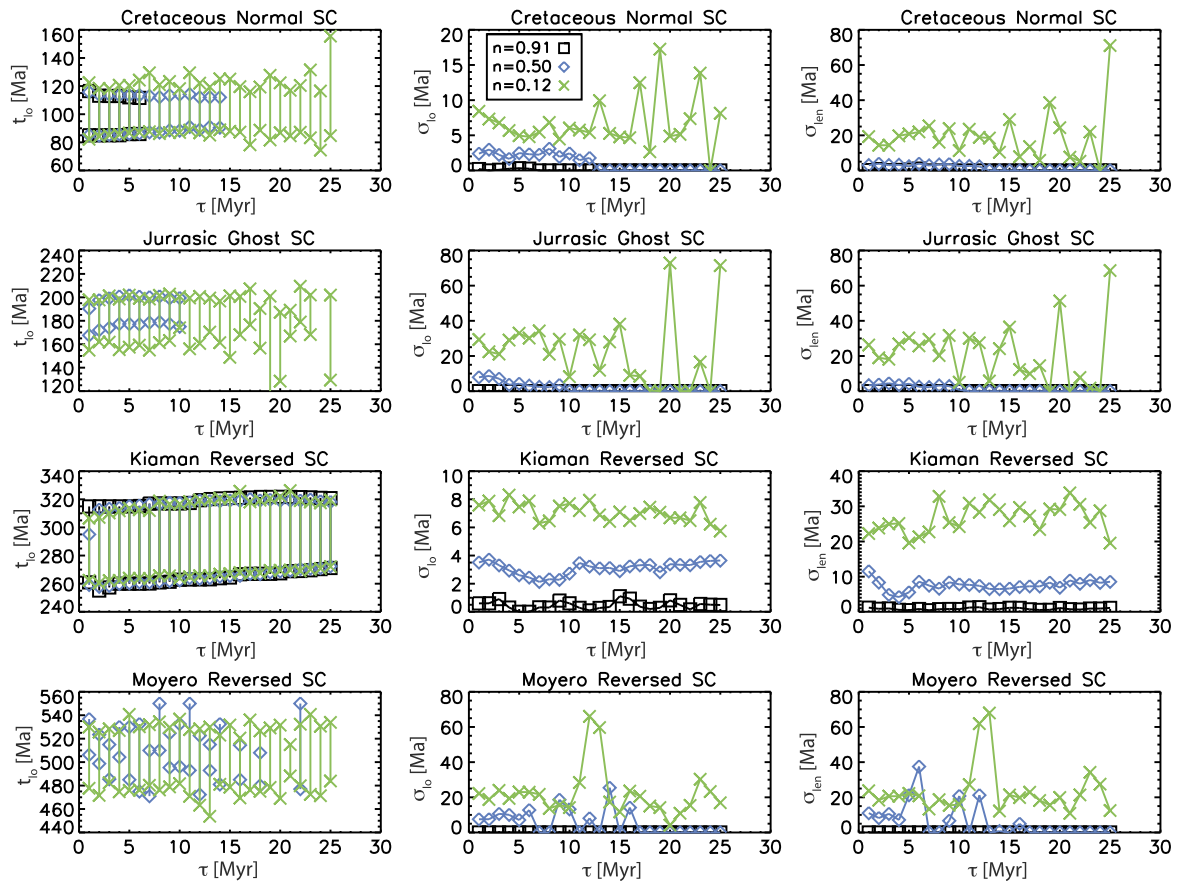| Superchron name	N_{SC}	Mean t_{lo} (σ_{lo})	Mean t_{len} (σ_{len})	Mean age	Age for $\tau = 1$	Age for $\tau = 7$
Keweenawan N	7	1055 (0)	38 (4)	1055–1093	1055–1098	1055–1087
Middle Gardar N	19	1151 (10)	108 (36)	1151–1259	1122–1200	1150–1299
MacKenzie N	23	1170 (20)	115 (21)	1170–1286	0	1150–1299
Middle Belt R	5	1420 (4)	19 (4)	1420–1439	1425–1443	0
Lower Belt N	5	1458 (1)	17 (1)	1458–1476	1457–1476	0
Upper McArthur R	9	1589 (1)	24 (1)	1589–1613	1589–1614	1589–1614
Middle McArthur R	1	1633 (0)	19 (0)	1633–1652	1633–1652	0
Cleaver N	1	1769 (0)	16 (0)	1769–1785	1769–1785	0
Sudbury N	1	1838 (0)	25 (0)	1838–1863	1838–1863	0
Superior R	25	2051 (30)	46 (35)	2051–2098	1998–2105	2069–2105
Superior N	7	2125 (0)	45 (0)	2125–2170	2125–2170	2125–2170

Fig. 3. Statistical superchron occurrence for a range of smoothing windows τ and sampling densities n_{samp} (in units of samples per Myr) of $n_{samp} = 0.91$ (black square, corresponding to the full Phanerozoic data set), $n_{samp} = 0.5$ (blue diamond), and $n_{samp} = 0.12$ (green 'x', similar to the Proterozoic sampling rate). Each point denotes the result of 100 bootstraps of the Phanerozoic data set. Shown for each superchron are the mean ending age t_{lo} and time span $t_{lo} + t_{len}$ (left column), standard deviation of ending age σ_{lo} (center column), and standard deviation of superchron length σ_{len} (right column). Rows show the Cretaceous Normal Superchron (first), Jurassic Ghost Superchron (second), Kiaman Reversed Superchron (third), and Moyero Reversed Superchron (fourth). Note the vertical range of axes varies. (For interpretation of the references to color in this figure legend, the reader is referred to the web version of this article.)

tion of the ending age of the CNS is somewhat higher than that of the KRS, but typically around $\sigma_{lo} \sim 10$ Myr.

The Moyero, the most elusive superchron, is not identified with a high sampling density ($n_{samp} = 0.91$ Myr^{-1}) and is only sporadically identified at medium sampling density ($n_{samp} = 0.5$ Myr^{-1}) (Fig. 3). At low sampling density the MRS is identified for all τ but the deviation of the ending age is high, with $\sigma_{lo} \sim 20$ Myr, and even higher for some τ. The JGS is falsely identified about as often as the real MRS is correctly identified. However, there are three main differences between the JGS and MRS: (1) identification of the MRS is more consistent as a function of τ than the JGS, which occurs sporadically, (2) the MRS is found more often with medium sampling density (17 versus 10, Table 2), and (3) the deviation of the ending age and length of the MRS ($\sigma_{lo} \sim 20$ Myr, $\sigma_{len} \sim 25$ Myr) is typically lower than those of the JGS ($\sigma_{lo} \sim 30$ Myr, $\sigma_{len} \sim 35$ Myr).

3.2. Proterozoic

Similar to the Phanerozoic analysis, the Proterozoic polarity ratio sequence (Fig. 2(right)) is analyzed over a range of smoothing windows from $\tau = 1$ to 25 Myr (Table 3, Fig. 4). In this analysis all Proterozoic data is included (i.e. no bootstrapping), which implies a sampling density of $n_{ave} = 0.12$ Myr^{-1}. All Proterozoic chrons longer than 15 Myr are assigned a name according to their dominant site name. Additionally, if a Proterozoic chron includes the mean of the age range of a named superchron then the chron is assigned that name.
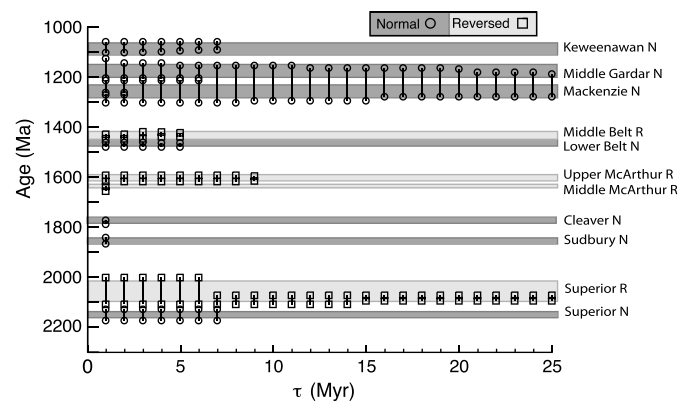

Fig. 4. Sensitivity of estimated Proterozoic superchrons to smoothing parameter τ. Normal (reversed) chrons are labeled with circles (squares) and dark (light) shading.

Fig. 4 and Table 3 summarize the number of times each superchron is identified (out of 25) and the mean ending age and length. We note that the range of smoothing window sizes is arbitrary, but since Phanerozoic polarity statistics are relatively stable up to $\tau = 25$ we are encouraged to use the same for the Proterozoic. The timing and occurrence of each superchron is sensitive to smoothing window size τ, so that small τ lends to more numerous and shorter duration superchrons, while large τ lends towards less in number and longer duration superchrons. In particular, the Middle Gardar N (1150–1240 Ma) and Mackenzie N (1183–1272 Ma)

events are smeared into a single 100 Myr long superchron for $\tau > 10$ Myr (Fig. 4). Although the combined Mackenzie and Gardar Superchrons are robustly identified at all τ, it is not clear whether to interpret them as two separate events or one long superchron because the polarity ratio is greater than 50% normal for the combined age range (1122–1291 Ma). The other robustly identified Proterozoic superchron is the Superior R (2051–2097 Ma), which is identified at all τ, but has a poorly constrained mean length of $t_{len} = 46 \pm 35$ Myr.

Other identified Proterozoic superchrons include the Keweenawan N (1055–1092 Ma), the Middle Belt R (1420–1439 Ma), the Lower Belt N (1458–1475 Ma), and the Upper McArthur R (1589–1613 Ma), each identified at 28%, 20%, 20%, and 36% of the τ values, respectively.

For comparison, the same analysis was repeated for a shorter required minimum superchron length of 10 Myr, which yields more superchrons of shorter duration. In particular, analysis with this more liberal definition identifies the Maya N twice, the Keweenawan R once, the Cleaver N twelve times, and the Sudbury N five times out of 25 τ cases. All other superchrons are identified similar to Table 3, indicating our nominal choice of superchron length (15 Myr) produces more conservative results.

Generally the Proterozoic polarity ratio dataset shows similar response to varying τ as the Phanerozoic analysis: at lower τ, more superchrons are indicated; whereas for $\tau > 10$ fewer apparent superchrons are recognized, with larger variation in estimated durations and starting/ending times (Fig. 4, Table 3). At extreme τ, apparent superchrons with ultra long durations of more than 100 Myr may indicate artifacts in the sparse dataset. Values of τ in the range of 5–9 Myr largely avoid such artifacts, and indicate 3–8 superchrons through the 1300 Myr interval analyzed (Table 3). Among those, three (Keweenawan N, Middle Belt R, McArthur R) were previously recognized by magnetostratigraphic studies (Davis and Green, 1997; Elston et al., 2002; Idnurm et al., 1995). Among the others, three are stable across a range of τ values (Middle Gardar N, Mackenzie N, Superior R; the former two amalgamated for $\tau \geq 7$), and two are only revealed for $\tau \leq 7$ (Lower Belt N, Superior N). Two other Proterozoic superchrons were postulated previously (Maya N, Cleaver N), as noted above, but are not recovered by our analysis at the optimal range of τ due to low representation in the quality-filtered database.

4. Conclusions

In summary, values of τ in the range of 5–10 Myr adequately reproduce the principle behavior of polarity bias through Phanerozoic time (Fig. 3), even at subsampling rates comparable to the sparse Proterozoic database. In total, we identify 3–10 possible superchrons through a 1300 Myr interval of Proterozoic time, which are broadly comparable in frequency to those of the Phanerozoic appearing at circa 200 Myr recurrence. As more Proterozoic paleomagnetic data are acquired, some of our proposed superchrons may disappear while others may appear; however, at present there is no reason to expect estimated Proterozoic superchron frequency to change dramatically.

The major implication of this observation is that the geodynamo has occupied a quasi-stationary reversal state, fluctuating from weak to strong polarity bias, for more than a billion years. Stable fluctuation in polarity reversal frequency over the last two billion years implies either (i) that polarity reversals in general are largely insensitive to core evolution or (ii) a remarkably stable evolution of core dynamics over this time, where buoyancy and rotation forces are roughly in balance. The former hypothesis seems unlikely given that numerical dynamos have revealed sensitivity of dipole reversal rate to the energetic state of the core: with both faster core cooling rates (Driscoll and Olson, 2011) and equa-

torial core–mantle boundary cooling patterns (Olson et al., 2015) leading to increased polarity reversal frequency. On the contrary, the later may imply that the geodynamo has evolved through a relatively narrow dynamo regime, and that inner core nucleation ca. 600 Ma did not permanently disrupt the reversing state of the geodynamo. Instead, inner core nucleation may have caused only a temporary disruption to the dipolar nature of the field, complicating the late Neoproterozoic APWPs (Raub et al., 2007; Halls et al., 2015). Another remote possibility is that the inner core is much older (> 2 Ga), whereby its slow growth has allowed a stable geodynamo state to persist, with periods of frequent reversals bounded by periods of strong polarity bias or superchrons. Connecting Phanerozoic reversal rates to reconstructed mantle convection has proved challenging (Olson et al., 2015); hinting at the difficulty of connecting similar events in the Proterozoic.

Two additional intriguing features of our Proterozoic polarity bias analysis emerge. First, at all levels of averaging, N polarity appears more abundantly than R polarity, in both the global dataset (Fig. 2(right)), where the mean polarity ratio is 57%, and in the estimation of superchrons (Fig. 4). This feature was noted previously (Irving and Pullaiah, 1976; Roberts and Piper, 1989) on more limited or quality-unfiltered datasets. Assignment of N absolute polarity to this pronounced long-term bias hinges chiefly on the orography of paleowind directions across Laurentia, as noted above, but the predominance of one polarity over the other remains even if that constraint is removed. As the dynamo equations have no preferred polarity, this bias implies either a prolonged magnetic boundary heterogeneity (at the ICB or CMB) or a long-term magnetic memory in the core.

Second, there is as yet no obvious relationship between superchron occurrence and phases of a postulated supercontinent cycle. The Rodinia interval (900–700 Ma) was excluded from our analysis because of poor APWP connectivity among various cratons, but the Nuna interval (1600–1300 Ma) and adjacent periods are relatively well represented by data. Depending on one's choice of τ, the Nuna interval may have experienced one or several superchrons, and thus may or may not be comparable to the Pangea interval with its single superchron (Kiaman R). The geodynamo was frequently reversing during initial stages of Nuna assembly (1900–1800 Ma), but the following interval of initial Rodinia assembly (1100–1000 Ma) witnessed perhaps one or two N superchrons. Difficulty in relating patterns of mantle convection to geodynamo reversal state in Proterozoic time is reminiscent of the difficulty in explaining the Cretaceous N superchron during a period of globally high seafloor spreading rates, subduction, and thus core heat flow (Biggin et al., 2012; Olson et al., 2015). Ultimately, association of long-term geodynamo behavior to modes of mantle convection must await augmentation of the Proterozoic paleomagnetic database, but the methods described herein are readily suited for analysis of that expanded future record.

Appendix A. Smoothing function

Polarity ratio data is smoothed using the inverse distance squared weighting function as described by Algeo (1996). Provided a sequence of polarity ratios P_i at ages A_i, where i is the index of paleomagnetic unit sampled, the weight factor $\Gamma_i(t)$ of unit i as a function of time t is

$$\Gamma_i(t) = \frac{1}{\left(\frac{A_i - t}{\tau}\right)^2 + 1} \tag{A.1}$$

where τ is the smoothing window size. The running mean polarity ratio $P_{ave}(t)$ is

$$P_{ave}(t) = \frac{\sum_i^N P_i \Gamma_i(t)}{\sum_i^N \Gamma_i(t)} \tag{A.2}$$

where N is the total number of paleomagnetic units. The standard deviation of the running mean σ_P is

$$\sigma_P = \left[\frac{\sum_i^N (P_i - P_{ave}(t))^2 \Gamma_i(t)}{\sum_i^N (\Gamma_i(t) - 1)} \right]^{1/2} \tag{A.3}$$

where we have corrected a typo in the original form (equation (3) in Algeo, 1996). This smoothing function is applied to the polarity ratio sequences and the running mean polarity ratio $P_{ave}(t)$ and standard deviation σ_P are plotted in Fig. 2.

Appendix B. Supplementary material

Supplementary material related to this article can be found online at http://dx.doi.org/10.1016/j.epsl.2015.12.035.

References

Abrajevitch, A., Van der Voo, R., 2010. Incompatible Ediacaran paleomagnetic directions suggest an equatorial geomagnetic dipole hypothesis. Earth Planet. Sci. Lett. 293 (1), 164–170.
Algeo, T.J., 1996. Geomagnetic polarity bias patterns through the Phanerozoic. J. Geophys. Res. 101 (B2), 2785–2814.
Biggin, A., Steinberger, B., Aubert, J., Suttie, N., Holme, R., Torsvik, T., van der Meer, D., van Hinsbergen, D., 2012. Possible links between long-term geomagnetic variations and whole-mantle convection processes. Nat. Geosci. 5 (8), 526–533.
Blackburn, T.J., Olsen, P.E., Bowring, S.A., McLean, N.M., Kent, D.V., Puffer, J., McHone, G., Rasbury, E.T., Et-Touhami, M., 2013. Zircon U–Pb geochronology links the end-Triassic extinction with the Central Atlantic Magmatic Province. Science 340 (6135), 941–945.
Buchan, K.L., 2013. Key paleomagnetic poles and their use in Proterozoic continent and supercontinent reconstructions: a review. Precambrian Res. 238, 93–110.
Burgess, S., Bowring, S., Fleming, T., Elliot, D., 2015. High-precision geochronology links the Ferrar large igneous province with early-Jurassic ocean anoxia and biotic crisis. Earth Planet. Sci. Lett. 415, 90–99.
Coe, R., Glatzmaier, G., 2006. Symmetry and stability of the geomagnetic field. Geophys. Res. Lett. 33, L21311 (5).
Davis, D., Green, J., 1997. Geochronology of the North American Midcontinent rift in western Lake Superior and implications for its geodynamic evolution. Can. J. Earth Sci. 34 (4), 476–488.
Driscoll, P., Olson, P., 2011. Superchron cycles driven by variable core heat flow. Geophys. Res. Lett. 38 (9), L09304.
Elston, D., Enkin, R., Baker, J., Kisilevsky, D., 2002. Tightening the Belt: paleomagnetic–stratigraphic constraints on deposition, correlation, and deformation of the Middle Proterozoic (ca. 1.4 Ga) Belt-Purcell Supergroup, United States and Canada. Geol. Soc. Am. Bull. 114 (5), 619–638.
Gallet, Y., Pavlov, V., Halverson, G., Hulot, G., 2012. Toward constraining the long-term reversing behavior of the geodynamo: a new "Maya" superchron 1 billion years ago from the magnetostratigraphy of the Kartochka Formation (southwestern Siberia). Earth Planet. Sci. Lett. 339, 117–126.
Gradstein, F.M., Ogg, J.G., Smith, A.G., Bleeker, W., Lourens, L.J., 2004. A new geologic time scale, with special reference to Precambrian and Neogene. Episodes 27 (2), 83–100.
Halls, H.C., Lovette, A., Hamilton, M., Söderlund, U., 2015. A paleomagnetic and U–Pb geochronology study of the western end of the Grenville dyke swarm: rapid changes in paleomagnetic field direction at ca. 585 Ma related to polarity reversals? Precambrian Res. 257, 137–166.
Hoffman, P.F., Grotzinger, J.P., 1993. Orographic precipitation, erosional unloading, and tectonic style. Geology 21 (3), 195–198.
Idnurm, M., Giddings, J., Plumb, K., 1995. Apparent polar wander and reversal stratigraphy of the Palaeo-Mesoproterozoic southeastern McArthur Basin, Australia. Precambrian Res. 72 (1), 1–41.
Irving, E., Baker, J., Hamilton, M., Wynne, P., 2004. Early Proterozoic geomagnetic field in western Laurentia: implications for paleolatitudes, local rotations and stratigraphy. Precambrian Res. 129 (3), 251–270.
Irving, E., McGlynn, J., Morgan, G., 1976. Proterozoic magnetostratigraphy and the tectonic evolution of Laurentia [and discussion]. Philos. Trans. R. Soc., Math. Phys. Eng. Sci. 280 (1298), 433–468.
Irving, E., Pullaiah, G., 1976. Reversals of the geomagnetic field, magnetostratigraphy, and relative magnitude of paleosecular variation in the Phanerozoic. Earth-Sci. Rev. 12 (1), 35–64.
Johnson, H.P., Van Patten, D., Tivey, M., Sager, W.W., 1995. Geomagnetic polarity reversal rate for the Phanerozoic. Geophys. Res. Lett. 22 (3), 231–234.
Li, J., Ge, K., Pan, Y., Williams, W., Liu, Q., Qin, H., 2013. A strong angular dependence of magnetic properties of magnetosome chains: implications for rock magnetism and paleomagnetism. Geochem. Geophys. Geosyst. 14 (10), 3887–3907.
Lowrie, W., Kent, D., 2004. Geomagnetic polarity timescales and reversal frequency regimes. In: Chapman Conference on Timescales of the Internal Geomagnetic Field. Gainesville, Florida. In: Geophys. Monogr. Ser., vol. 145, pp. 117–129.
McElhinny, M.W., 1971. Geomagnetic reversals during the Phanerozoic. Science 172 (3979), 157–159.
Ogg, J., 2012. The geomagnetic polarity time scale, Ch. 5. In: The Geologic Time Scale. Elsevier, pp. 85–114.
Olson, P., Deguen, R., Rudolph, M.L., Zhong, S., 2015. Core evolution driven by mantle global circulation. Phys. Earth Planet. Inter. 243, 44–55.
Pavlov, V., Gallet, Y., 2005. A third superchron during the early Paleozoic. Episodes 28 (2), 78–84.
Pavlov, V., Gallet, Y., 2010. Variations in geomagnetic reversal frequency during the Earth's middle age. Geochem. Geophys. Geosyst. 11 (1).
Pehrsson, S.J., Eglington, B.M., Evans, D.A., Huston, D., Reddy, S.M., 2015. Metallogeny and its link to orogenic style during the Nuna Supercontinent Cycle. Geol. Soc. Lond. Special Publ., vol. 424, SP424-5.
Pisarevsky, S.A., Elming, S.-Å., Pesonen, L.J., Li, Z.-X., 2014. Mesoproterozoic paleogeography: supercontinent and beyond. Precambrian Res. 244, 207–225.
Raub, T., Kirschvink, J., Evans, D., 2007. True polar wander: linking deep and shallow geodynamics to hydro- and bio-spheric hypotheses. In: Treatise on Geophysics, vol. 5, pp. 565–589.
Roberts, N., Piper, J., 1989. A description of the behavior of the Earth's magnetic field. In: Geomagnetism, vol. 3. Academic Press, London, pp. 163–260.
Torsvik, T.H., Van der Voo, R., Preeden, U., Mac Niocaill, C., Steinberger, B., Doubrovine, P.V., van Hinsbergen, D.J., Domeier, M., Gaina, C., Tohver, E., et al., 2012. Phanerozoic polar wander, palaeogeography and dynamics. Earth-Sci. Rev. 114, 325–368.
Veikkolainen, T., Pesonen, L.J., Evans, D.A., 2014. PALEOMAGIA: a PHP/MYSQL database of the Precambrian paleomagnetic data. Stud. Geophys. Geod. 58 (3), 425–441.